Energy Analysis of Hydraulic Fracturing

Aliakbar Golshani* and Thanh Tran-Cong**

*Lecturer, Faculty of Engineering and Surveying, University of Southern Queensland, Toowoomba, QLD 4350, Australia (E-mail: golshani@usq.edu.au)

**Lecturer, Faculty of Engineering and Surveying, University of Southern Queensland, Toowoomba, QLD 4350, Australia (E-mail: trancong@usq.edu.au)

Abstract
In this paper, numerical simulations of circular boreholes under internal hydraulic pressure are carried out to investigate the energy transferred to the surrounding rock and the breakdown pressure. The simulations are conducted by using a micromechanical continuum damage model proposed by Golshani et al. (2006). The simulation results suggest that the borehole breakdown pressure and the energy transferred to the surrounding rock are dependent on the mechanical properties of the rock and borehole size. Although the energy transferred to the surrounding rock increases with increasing borehole size, the borehole breakdown pressure decreases.

Keywords: Hydraulic Fracturing, Micromechanics, Numerical Modelling

1. Introduction
Stresses are applied inside the boreholes either to produce deformations in order to determine the modulus of the rock or to induce fractures (Jaeger and Cook, 1969). Hydraulic fracturing is one of the techniques used to stimulate the production of oil or gas in reservoirs. This technique involves pumping a fluid under pressure into a borehole. This pressurized fluid introduced into the borehole produces stress concentration in the surrounding rock causing the development of fractures. Other applications of hydraulic fracturing have been recently found in geotechnical engineering for ground reinforcement and in environmental engineering for solid waste disposal. In fact, attention is focused on the prediction of the borehole pressure and is usually the only parameter available to evaluate the operation (Papanastasiou, 1997). However, the energy transferred to the rock during pressurization of the borehole can be considered as another parameter for the evaluation of the operation.

Energy can be stored in or released from the rock medium in the vicinity of a borehole subjected to internal pressure. If the internal energy exceeds the limit that the material can withstand, the energy release will occur to re-establish the internal energy level within a tolerable limit. Griffith (1920) suggested that a potential relief mechanism is the microcracking. According to his theory the excess of energy is dissipated with the growth of microcracks during rock failure.

The energy transferred to the surrounding rock associated with the phenomena occurring in the borehole under breakdown pressure (the energy requirements for rock fracturing) is given by

$$W = W_s + W_f + W_t + W_c \tag{1}$$

where W_s, W_f, W_t and W_c represent strain energy (borehole wall deformation), fracture energy, thermal energy (thermal exchange between rock and fluid) and chemical energy (chemical change of the rock due to the interaction with the fluid).

The strain energy is the potential energy stored in the rock under stress and is given by

$$W_s = \frac{1}{2}\int_V \sigma : \varepsilon \ dV \tag{2}$$

where V is the volume of the rock. σ and ε are the stress and strain in the rock under applied stresses. The symbol (:) stands for the inner product.

The fracture energy is material property of rock and is given by

$$W_f = \frac{K_c^2}{E} A \tag{3}$$

where K_C and E are the fracture toughness and Young's modulus of the rock and A is the area of fracture created.

When the internal energy reaches a critical limit, this level must be reduced by one or more relief mechanisms. As previously explained, the most significant relief mechanism for rocks is microcracking.

The main objective of this paper is to investigate numerically the energy transferred to the rock around a vertical borehole under breakdown pressure i.e., the pressure at which fracturing occurs, by using a micromechanics-based continuum damage model (2D) proposed by Golshani et al. (2006). For this purpose three types of rocks i.e., Inada granite, Mount Isa granite and Toowoomba basalt are simulated. The effect of borehole diameter on the transferred energy will also be discussed. In this study we only consider the effects of borehole wall deformation and the fracture energy and the fluid is restricted from entering the microcracks.

2. Micromechanics-based continuum damage model

In this model, the rock matrix is regarded as an elastic solid with N groups of microcracks distributed at different orientations, and the i-th group is characterized by the microcracks orientation $\theta^{(i)}$, the number density of the microcracks $\rho^{(i)}$, and the average microcracks length $2c^{(i)}$. $\theta^{(i)}$ is the inclination angle of the unit vector $n^{(i)}$, normal to a microcrack, to the global axis x_1 (see Fig. 1). In the following discussion, "'" indicates quantities in the local coordinate x'_i- axes.

By assuming that microcrack growth occurs in tensile mode I (Hallbauter et al., 1973, Kranz, 1979, Costin, 1983, Blair and Cook, 1998), the stress intensity factor K_I for a single microcrack with respect to local axes x'_i ($i=1, 2$) axes is approximated by

$$K_I = -\sqrt{\pi c} \ \sigma'_t \tag{4}$$

where σ'_t is the tensile stress acting normal to the microcrack surface (Fig. 2), and is expressed as:

$$\sigma'_t = \sigma'_{22} + (d/c)S'_{22} \tag{5}$$

Where S'_{22} is the deviatoric stress $(= (\sigma'_{22} - \sigma'_{11})/2)$.

It should be noted that the compressive stress is taken to be positive. The first term on the right hand side of Eq (5) stems from the far field compression, hence it takes a positive value (compression) in a common case. This means that the first term acts as an inhibiting factor for microcracking. The second term is the tensile stress, which is locally generated as a result of the inhomogeneity of rock and sliding movement on asperities. Following the suggestion by

Costin (1983), we assume that the local tensile stress increases proportionally to the deviatoric stress S'_{22}. d is a typical length scale of material such as grain size, and is experimentally determined (see Golshani et al., 2006). It is of particular importance to point out that the local tensile stress decreases as the microcrack grows. Otherwise, the microcrack would propagate without any limit as soon as the stress intensity factor K_I reaches the fracture toughness K_{IC}.

The stress-induced microcrack growth takes place in tensile mode I when the following relation is satisfied

$$K_I - K_{IC} = -\sqrt{\pi c} \; \sigma'_t - K_{IC} = 0 \tag{6}$$

Eq (6) was formulated for a single microcrack and the effect of neighbouring microcracks was not considered. In order to evaluate the elastic interaction among neighbouring microcracks, we use the so-called pseudo-traction method developed by Horii and Nemat-Nasser (1985a, 1985b). For simplicity, we first consider an infinite plate with two microcracks α and β with lengths $2c_\alpha$ and $2c_\beta$, both of which are subjected to far field stresses (see Fig. 3). This problem is elastically analysed by decomposing it into three sub-problems; i.e. a homogeneous sub-problem and two sub-problems α and β, as shown in Figure 3. There is no microcrack in the homogenous sub-problem, which is subjected to the same far field stresses as the original problem (i.e. σ_{11}, σ_{22} and σ_{12}). In the sub-problem α and β, we deal with a single microcrack under zero stresses, individually. The traction-free condition must be satisfied on the surface of the microcracks in the original problem since the microcracks α and β are assumed to be open. To do this, $-(\sigma'^{\alpha}_{22} + \sigma'^{P\alpha}_{22})$ and $-(\sigma'^{\alpha}_{12} + \sigma'^{P\alpha}_{12})$ must be applied to the surface of the microcrack α in the sub-problem α. Here, σ'^{α}_{22} and σ'^{α}_{12} are the stresses at the position of microcrack α arising from the far field stresses in the homogenous problem, and $\sigma'^{P\alpha}_{22}$ and $\sigma'^{P\alpha}_{12}$, called pseudo-tractions, stand for the stresses at the position of microcrack α in sub-problem β. That is, the pseudo-tractions are generated by microcrack β through elastic interactions between the microcracks α and β.

The pseudo-tractions are calculated such that all the boundary conditions for the original problem are satisfied

$$\{\sigma'^{P\alpha}\} = \lfloor \gamma'^{\alpha\beta} \rfloor (\{\sigma'^{\beta}\} + \{\sigma'^{P\beta}\}) \tag{7}$$

where $\{\sigma'^{P\alpha}\} = \{\sigma'^{P\alpha}_{11}, \sigma'^{P\alpha}_{22}, \sigma'^{P\alpha}_{12}\}^T$, $\{\sigma'^{\beta}\} = \{\sigma'^{\beta}_{11}, \sigma'^{\beta}_{22}, \sigma'^{\beta}_{12}\}^T$, and $\lfloor \gamma'^{\alpha\beta} \rfloor$ is a 3×3 matrix and each element of which is a function of the position vectors x^α and x^b of the centres of microcracks α and β, their half lengths (c_α and c_β), and the inclination angle $\theta_{\alpha\beta}$ between $x_1'^{\beta}$ and $x_1'^{\alpha}$. Eq (7) is tentatively called the consistency equation in the sense that stress boundary conditions are taken into account. If more details are necessary, readers should refer to the papers by Horii and Nemat-Nasser (1985a, 1985b), Okui et al. (1993), and Golshani et al. (2006).

Considering the effect of the interaction among microcracks, the stress intensity factor equation (Eq (4)) can be rewritten as follows

$$K_I(\sigma', \sigma'^P, c) = -\sqrt{\pi c} \left[(\sigma'_{22} + \sigma'^P_{22}) + (d/c) \left(\frac{(\sigma'_{22} + \sigma'^P_{22}) - (\sigma'_{11} + \sigma'^P_{11})}{2} \right) \right] \tag{8}$$

It is assumed that the rock matrix remains elastic in the entire process so that the inelastic deformation arises from opening of microcracks. Since the matrix is elastic, the stress-strain relationship is given by:

$$\sigma = D_e : (\varepsilon_t - \hat{\varepsilon}) \tag{9}$$

where D_e is the elastic modulus tensor, and the symbol (:) stands for the inner product. ε_t is the total strain tensor and $\bar{\varepsilon}$ is the inelastic strain tensor arising from the opening of microcracks. The inelastic strain arising from opening the *i*-th group microcracks is formulated in terms of the average length of microcracks $2c^{(i)}$, microcracks orientation $\theta^{(i)}$, number density of microcracks $\rho^{(i)}$, and the applied stresses σ (Golshani et al., 2006).

We now have governing equations for analysing stress-induced behaviour of brittle rock; i.e., microcrack growth law (7), Consistency Eqs. (8) and Constitutive Eqs. (9). Unknowns are σ, c and σ^p. The initial values of the unknowns are given by solving boundary value problems by using the stress-induced microcrack growth law. They correspond to a state just after the application of a load. Based on the finite element methods, we solved the governing equations on a numerical basis. Three-node triangular elements were used, in each of which the displacement, the interaction stresses and the length of the microcracks belonging to the *i*-th group are constant.

3. Numerical simulation

A single borehole in rock medium (3000mm×3000mm) was simulated and plane strain condition was assumed. First mesh convergence study was performed to determine the finite element mesh with satisfactory accuracy. For this purpose, Inada granite was considered. Then using this mesh, numerical simulation was carried out for three types of rocks i.e., Inada granite, Mt. Isa granite and Toowoomba basalt to determine the internal energy transferred to the surrounding rock under pressure inside the borehole at failure (using Eqs.1-3).

3.1 Mesh convergence study

In finite element modelling, a finer mesh typically results in a more accurate solution. However, as a mesh is made finer, the computation time increases. A mesh convergence study enables us to obtain an accurate solution with a mesh that is sufficiently dense and not too demanding of computing resources. To perform a mesh convergence study, first we create a mesh using the fewest, reasonable number of nodes and elements and analyse the model. Then, we re-create the mesh with a denser element distribution, re-analyse it and compare the results to those of the previous mesh. We keep increasing number of nodes and elements and re-analyse the model until the results converge satisfactorily within a given tolerance.

Inada granite is biotite granite from a quarry in Kasama, Ibaraki, Japan. Inada granite consists of coarse to medium grains of quartz, feldspar and biotite. The mean grain size of Inada granite is about 2.0 mm (Takemura et al., 2005). The Inada granite had 73 MPa Young's modulus, 0.23 Poisson's ratio and the approximate stress-strain curves are given in Fig. 4. Fracture toughness and length parameter for Inada granite were chosen as $K_{IC} = 2.50$ MPa$^{1/2}$ and $d = 0.34$ mm. The average length of microcracks and microcrack number density are c=0.5mm and $\rho = 0.21$ (see Golshani et al., 2006). The uniaxial compression strength of Inada granite was reported as 218 MPa (Takemura et al., 2005)

We considered seven cases of meshes as shown in Table 1. The borehole diameter was 50 mm for all cases. Uniform pressure was applied inside the hole for each case and internal energy under breakdown pressure was determined (Fig. 5). Note that the results were normalized using the reference energy (W_r) that was chosen as the energy for the first case. As shown in Fig. 5, the energy remains essentially the same from the 3rd case (i.e., the mesh with 326 elements) onwards. It is noteworthy that computational cost increases faster than mesh sizes. Thus, we chose the fourth case: a mesh with 195 nodes and 350 elements that satisfies the accuracy requirement of a minimum computational cost.

3.2 Calculation of the energy for Inada granite, Mt. Isa granite and Toowoomba basalt

Mt. Isa granite occurs in Northwest Queensland, Australia and its grain size is about *0.2 mm* (Geoscience report, Australia, 2001). Toowoomba basalt (South-eastern Queensland, Australia) is generally fine-grained, dark grey to black igneous rock. In most cases individual minerals cannot be recognized by the naked eye because of the fine grain size (Willmott et al., 1995). Basalt is characterized by mineral grain size less than *0.3 mm* and for Toowoomba basalt, which is fine-grained basalt, the average grain size is set to *0.05 mm*.

The input parameter used in the numerical simulation of Mt. Isa granite and Toowoomba basalt are listed in Table 2 where elastic properties and fracture toughness are from experimental tests using samples with 60 mm diameter and 145 mm height.

In crystalline rocks, it is assumed that grain boundaries act as the predominant source of stress concentrating flaws and that the initial microcrack lengths are of the order of the rock grain size (Eberhardt et al., 1999). Thus, we can estimate initial microcrack length of Mt. Isa granite and Toowoomba basalt based on their grain size. The microcrack number density of Mt. Isa granite and Toowoomba basalt are not reported and are set to be 0.21 on a tentative basis.

The region (3000mm×3000mm) with a hole of 50 mm diameter was meshed with 195 nodes and 350 elements (Fig. 6). Uniform stress was applied inside the borehole and the energy at failure for Inada granite, Mt. Isa granite and Toowoomba basalt was obtained as 4.5 KJ, 5.7 KJ and 7.3 KJ. The breakdown stresses of theses three types of rocks were 173 MPa, 204 MPa and 255 MPa. The relationship between borehole pressure and transferred strain energy of Mount Isa granite is shown in Fig. 7.

The tangential stress at the borehole surface was calculated as -62.5 MPa, -71.4 MPa and -85.6 MPa for Inada granite, Mt. Isa granite and Toowoomba basalt, respectively. These stresses considerably exceed the tensile strength of these rocks obtained experimentally. The reason is that the borehole breakdown does not take place even if the largest tangential stress at the borehole surface reaches the tensile strength of rock. In fact, it occurs when the initiated fracture becomes unstable (Morita et al., 1996). In relation to this point, Haimson and Fairhust (1970) and Guo et al. (1993) found out that the tensile strength obtained from the hydraulic fracturing test (i.e., the largest tangential stress at the borehole surface) and the tensile strength obtained from the Brazilian test were different.

3.3 The borehole diameter

To investigate the effect of the borehole size on the energy transferred to the surrounding rock under breakdown pressure, Inada granite with boreholes of 25 mm, 50 mm and 75 mm diameter was simulated. The number of elements for these three simulations respectively was 494, 350 and 426 that provide us accurate results. The results show that borehole breakdown pressure and energy are dependent on the borehole size (Table 3). The borehole breakdown pressure is higher for smaller diameter holes. Morita et al. (1995) obtained similar results in the laboratory tests on cubic Berea sandstone (76 cm×76 cm×76 cm) with holes of 10 mm and 38 mm diameters subjected to internal pressure and far field confining stresses. As the borehole diameter increases, the energy transferred to the surrounding rock increases which is due to increase of strain energy component with increasing borehole diameter. Cuss et al. (2003) obtained similar results in their experiments with sandstone.

4. Conclusion

A single borehole in rock medium under internal pressure was simulated using a micromechanical continuum damage model (Golshani et al., 2006). The numerical simulation

predicts that the borehole breakdown pressure and the energy transferred to the rock depend on the formation's mechanical properties and borehole size. It was found that although the energy transferred to the surrounding rock increases with increasing borehole size the borehole breakdown pressure decreases. Furthermore, the energy seems to increase faster than the decrease of the breakdown pressure.

It should be noted that thermal energy and chemical energy were neglected in the calculation of the energy transferred to the rock around a borehole under internal pressure. For more accurate results these should be taken into consideration.

5. Acknowledgment

References

Blair, S.C. and Cook, N.G.W., (1998), "Analysis of compressive fracture in rock using statistical techniques: Part I.A non-linear rule-based model", International Journal of Rock Mechanics and Mining Sciences 35, 837–848.

Costin, L.S. 1983. A microcrack model for the deformation and failure of brittle rock. Journal of Geophysical Research, 88, B11, 9485-9492.

Cuss, R.J., Rutter, E.H. and Holloway, R.F., (2003), "Experimental observations of the mechanics of borehole failure in porous sandstone", International Journal of Rock Mechanics and Mining Sciences 40, 747-761.

Eberhardt, E., Stimpson, B. and Stead, D., (1999), "Effects of grain size on the initiation and propagation thresholds of stress-induced brittle failures", Rock Mechanics and Rock Engineering 32(2), 81-99.

Golshani, A., Okui, Y., Oda, M. and Takemura, T., (2006), "A micromechanical model for brittle failure of rock and its relation to crack growth observed in triaxial compression tests of granite", Mechanics of Materials, 38, 287-303.

Griffith, A. A., (1920), "The phenomena of rupture and flow in solids", Phil. Trans. Roy. Soc. of London, A221, 169-198.

Guo, F., Morgenstern, N.R. and Scott, J.D., (1993), "Interpretation of hydraulic fracturing breakdown pressure", International Journal of Rock Mechanics & Mining Sciences & Geomechanics Abstracts, 30, 6, 617-626.

Haimson, B.C. and Fairhurst, C., (1970), "In situ stress determination at great depth by means of hydraulic fracturing", Proceeding of 11th U.S. Symposium of Rock Mechanics, Berkeley, CA, 559-584.

Hallbauer, D.K., Wagner, H. and Cook, N.G.W., (1973), "Some observations concerning the microscopic and mechanical behaviour of quartzite specimens in stiff, triaxial compression tests", International Journal of Rock Mechanics and Mining Sciences 10, 713–726.

Horii, H. and Nemat-Nasser S., (1985a), "Compression-induced microcrack growth in brittle solids: axial splitting and shear failure", Journal of Geophysical Research, 90, 3105-3125.

Horii, H. and Nemat-Nasser S., (1985b), "Elastic fields of interacting inhomogeneities", International Journal of Solids and Structures, 21, 731-7450.

Jaeger, J., Cook, N.G.W. and Zimmerman, R., (1969), Fundamentals of rock mechanics,

Blackwell publishing.

Kranz, R.L., (1979), "Crack growth and development during creep of Barre granite", International Journal of Rock Mechanics and Mining Sciences 16, 23–36.

Morita, N., Black, A.D. and Fuh, G.F., (1996), "Borehole breakdown pressure with drilling fluid-I. Empirical results", International Journal of Rock Mechanics & Mining Sciences & Geomechanics Abstract, 33, 39-51.

Nemat-Nasser, S. and Hori, M., (1993), "Micromechanics: overall properties of heterogeneous materials", North-Holland, Netherlands, 687.

Okui, Y., Horii, H. and Akiyama, N., (1993), "A continuum theory for solids containing microdefects", International Journal of Rock Mechanics & Mining Sciences & Geomechanics Abstracts, 31, 5, 735-749.

Papanastasiou, P., (1997), "The influence of plasticity in hydraulic fracturing", International Journal of Fracture, 84, 61-79.

Takemura, T., Golshani, A., Oda, M. and Suzuki, K., (2003), "Preferred orientation of open microcracks in granite and their relation with anisotropic elasticity", International Journal of Rock Mechanics and Mining Sciences, 40, 443-454.

Willmott, W.F., O'Flynn, M.L. and Stevens, N.C., (1995), "The Bunya Mountains", Geological Society of Australia Inc (QLD Div.).
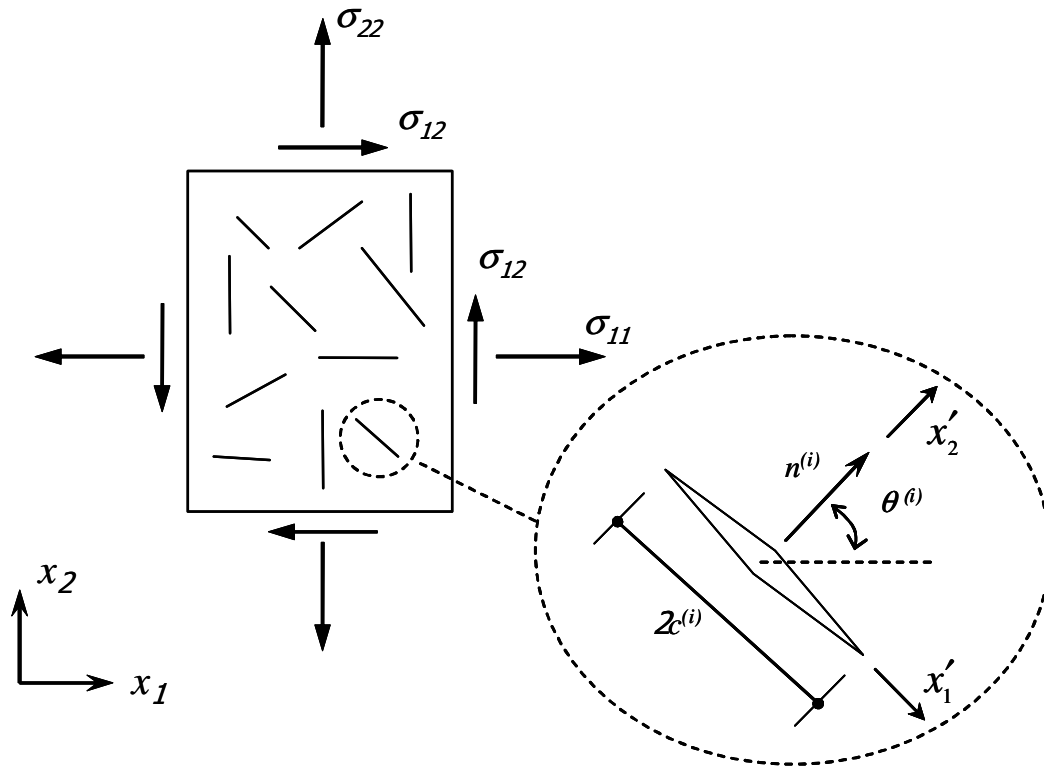
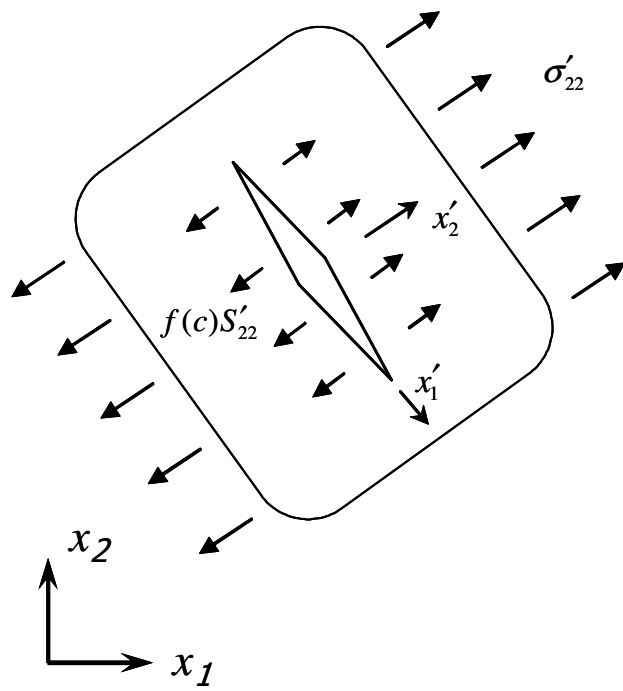Fig. 1. Rock material containing numerous microcracks
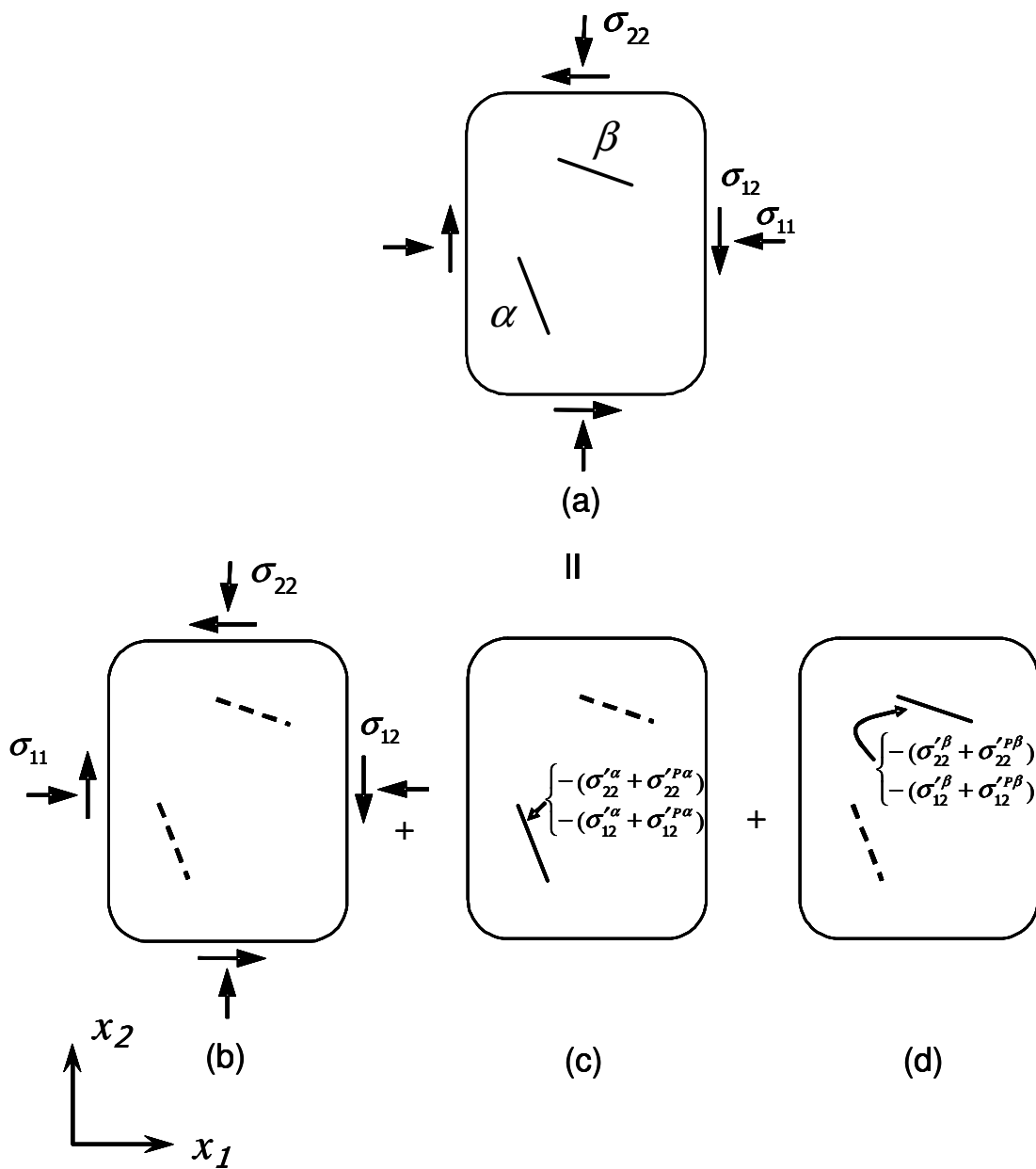
Fig. 2. A single microcrack under local stresses

Fig. 3. Decomposition of (a) the original problem into
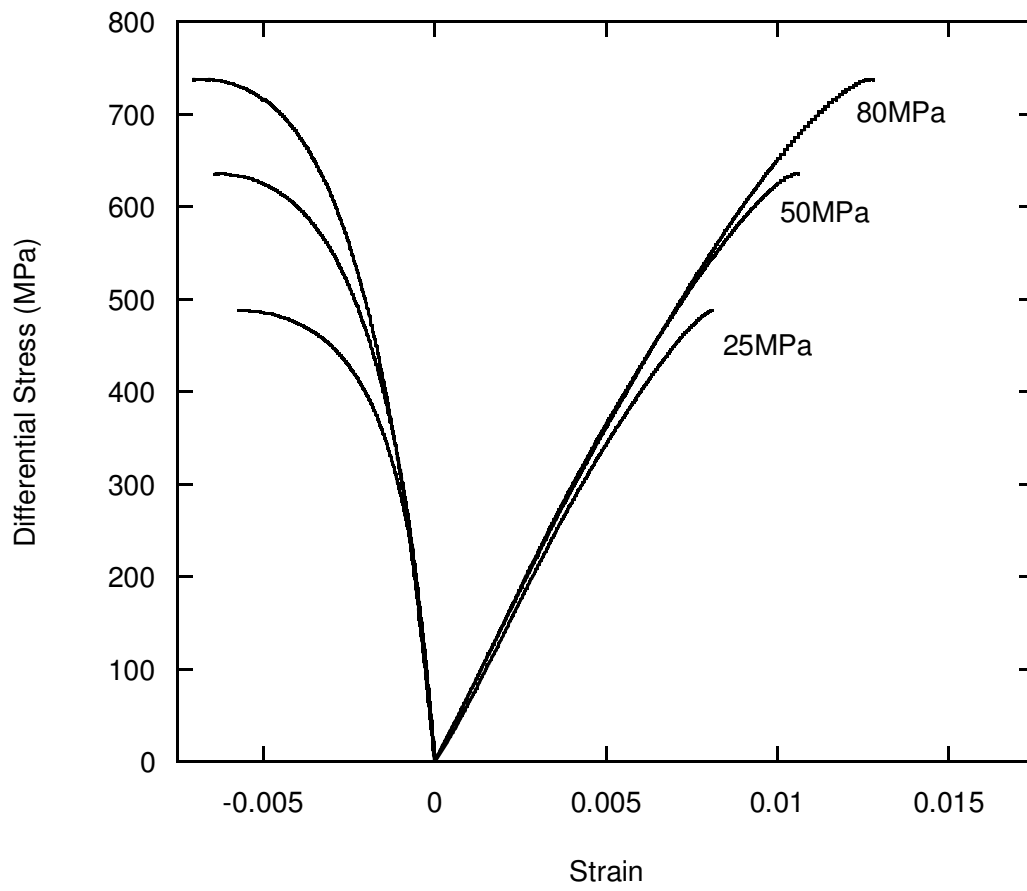(b) the homogeneous problem
and (c) and (d) two sub-problems

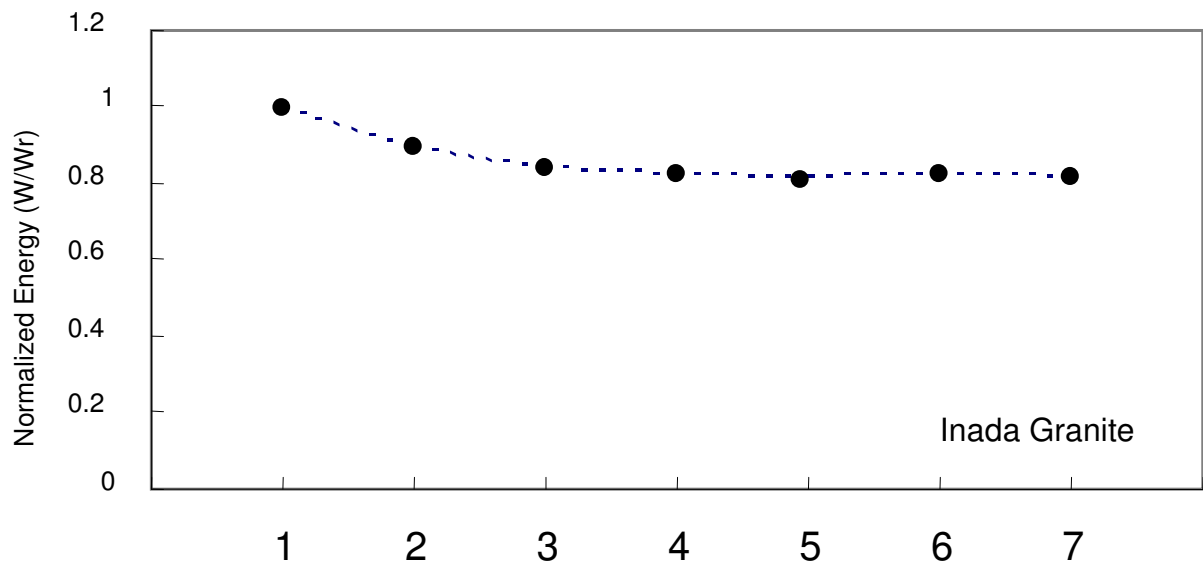Fig. 4. Stress strain curves for Inada granite

Fig. 5. Normalized energy for the meshes with different number of elements and nodes (Inada Granite)
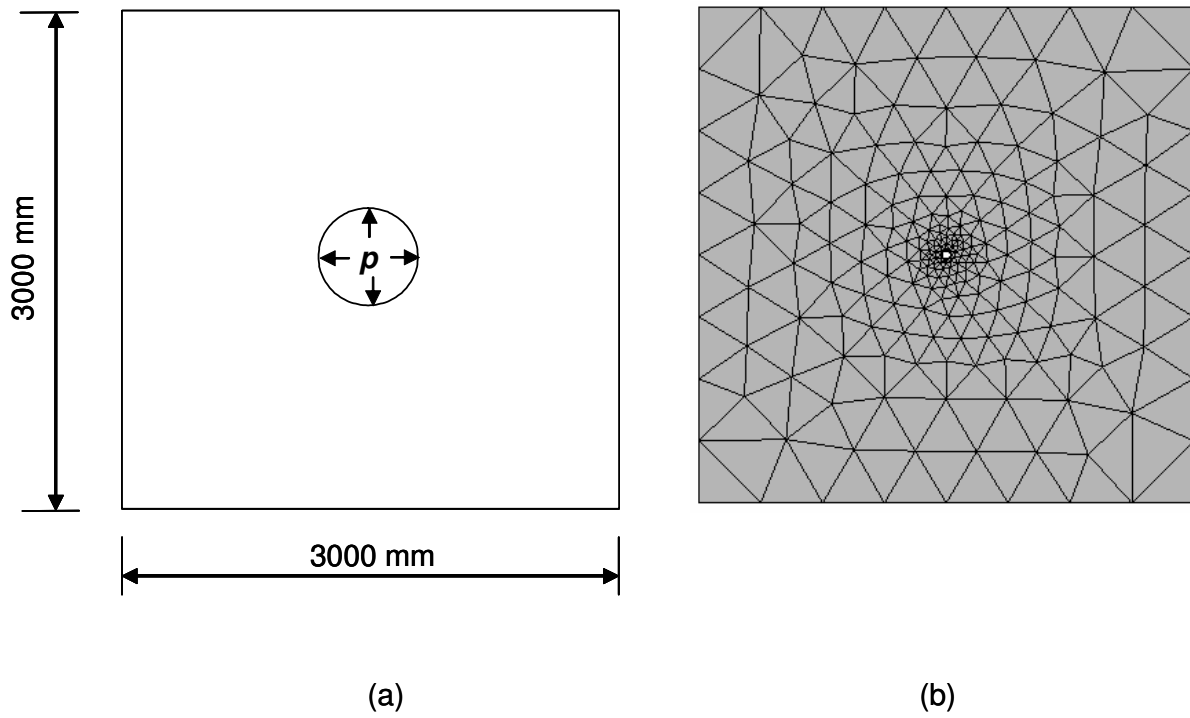
Figure 6. (a) A region with a hole inside under pressure of p (not scaled) (b) Finite element mesh
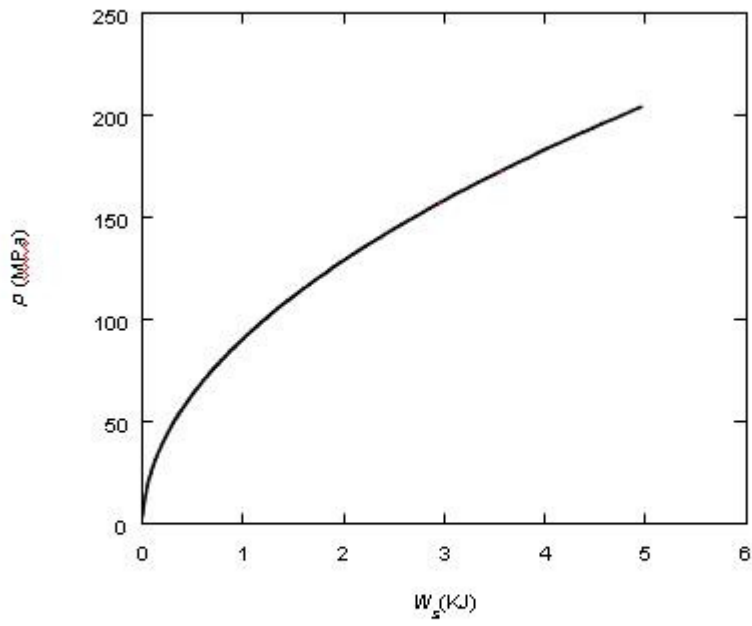
Fig. 7. Relationship between pressure *p* and strain energy *Ws* transferred to the surrounding

Table 1. Number of elements and nodes for different cases

Case No.	No. of elements	No. of nodes
1	234	132
2	246	140
3	326	182
4	350	195
5	414	228
6	510	278
7	626	338

Table 2. Model parameters used in numerical calculations for Mt. Isa Granite and Toowoomba Basalt

Parameter	Mt. Isa Granite	Toowoomba Basalt
Young's modulus (GPa)	61.4	78.7
Poisson's ratio	0.22	0.25
Fracture toughness (MPa m$^{1/2}$)	1.94	1.88
Initial microcrack length* (μm)	50	12.5
Number density of microcracks*	0.21	0.21
Tensile Strength (MPa)	-10.1	-14.8

* These data are estimates.

Table 3. Breakdown pressure and energy transferred to the surrounding rock at failure.

Hole diameter (mm)	Breakdown pressure (MPa)	Energy (KJ)
25	187	2.05
50	173	4.52
75	156	8.08